Supporting information

Asymmetric Lumino-Transformer: Circularly Polarized Luminescence of Chiral Eu(III) Coordination Polymer with Phase-Transition Behavior

Makoto Tsurui,[1] Yuichi Kitagawa,[2,3] Sunao Shoji,[2,3] Hitomi Ohmagari,[4] Miki Hasegawa,[4] Masayuki Gon,[5] Kazuo Tanaka,[5] Masato Kobayashi[3,6], Tetsuya Taketsugu[3,6], Koji Fushimi,[2] and Yasuchika Hasegawa*[2,3]

[1]Graduate School of Chemical Sciences and Engineering, Hokkaido University, Kita 13, Nishi 8, Kita-ku, Sapporo, Hokkaido 060-8628, Japan.

[2]Faculty of Engineering, Hokkaido University, Kita 13, Nishi 8, Kita-ku Sapporo, Hokkaido 060-8628, Japan.

[3]Institute for Chemical Reaction Design and Discovery (WPI-ICReDD), Hokkaido University, Kita 21, Nishi 10, Kita-ku, Sapporo, Hokkaido 001-0021, Japan.

[4]College of Science and Engineering, Aoyama Gakuin University, 5-10-1 Fuchinobe, Chuo-ku, Sagamihara, Kanagawa 252-5258, Japan

[5]Graduate School of Engineering, Kyoto University, Kyoto daigaku-katsura, Nishikyo-ku, Kyoto 615-8510, Japan.

[6]Faculty of Science, Hokkaido University, Kita 10, Nishi 8, Kita-ku, Sapporo, Hokkaido 060-0810, Japan.

Corresponding author footnote:

Tel. /Fax: +81-11-706-7114.

E-mail: hasegaway@eng.hokudai.ac.jp (Yasuchika Hasegawa)

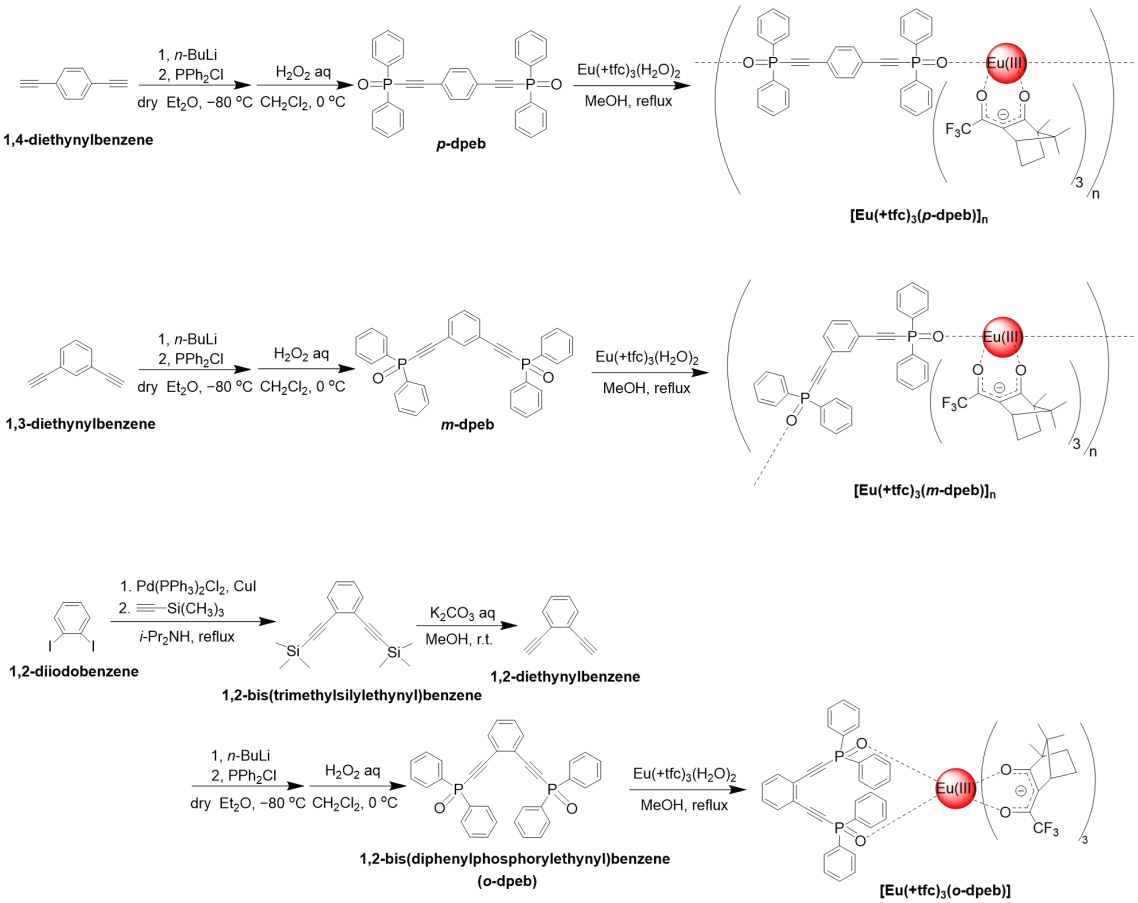

Scheme S1. Synthetic scheme of Eu(III) coordination polymers and complex.

Preparation of *o*-dpeb

o-dpeb was prepared with the procedure described in previous report.[S1] Trimethylsilylacetylene (3.9 mL, 28 mmol) was added in one portion to a degassed solution of 1,2-diiodobenzene (1.6 mL, 12 mmol), $Pd(PPh_3)_2Cl_2$ (0.37 g, 0.5 mmol), and CuI (0.40 g, 2.0 mmol) in diisopropylamine (80 mL) at room temperature. The mixture was refluxed under Ar atmosphere for 3 h. The reaction mixture was cooled to room temperature and ammonium salt was removed by filtration. Dichloromethane was added to the filtrate. The solution was washed with brine three times and dried over anhydrous $MgSO_4$. The solvent was evaporated, and the obtained black oil was purified by silica gel (Kanto Chemical, Silica gel 60N, 63-210 μm) column chromatography using hexane as an eluent to give 1,2-bis(trimethylsilylethynyl)benzene. The resulting 1,2-

bis(trimethylsilylethynyl)benzene (3.2 g, 12 mmol) was dissolved in methanol (34 mL), and 1 M K_2CO_3 aqueous solution (30 mL) was added. The mixture was stirred for 2 h at room temperature. The product was extracted with dichloromethane. The extracts were washed with brine three times and dried over anhydrous $MgSO_4$. The solvent was evaporated to afford 1,2-diethynylbenzene. The 1,2-diethynylbenzene (1.1 g, 8.6 mmol) was dissolved in dry diethyl ether (36 mL), and the mixture was degassed by Ar bubbling. A solution of *n*-BuLi (ca. 1.6 mol L^{-1}, 12 mL, 19 mmol) was added dropwise to the solution at −80 °C. The mixture was allowed to stir for 3.5 h at −10 °C, after which chlorodiphenylphosphine (3.4 mL, 19 mmol) was added dropwise at −80 °C. The mixture was gradually brought to room temperature and stirred for 24 h. The reaction mixture was poured into distilled water and extracted with dichloromethane. The extracts were washed with brine three times and dried over anhydrous $MgSO_4$. The solvent was evaporated, and the obtained black oil was placed with dichloromethane (10 mL) in a flask. The solution was cooled to 0 °C, and then a 30% hydrogen peroxide solution (16 mL) was added dropwise to the above solution. The solution was stirred for 3 h. After separation of aqueous hydrogen peroxide solution, the solution was washed with distilled water. Anhydrous $MgSO_4$ was added to the organic phases for dehydration. After filtration, the organic phase was evaporated to give brown powder. The obtained powder was purified by silica gel column chromatography using ethyl acetate as an eluent to afford white powder. Yield: 1.25 g (2.4 mmol, 20%). ^{1}H NMR ($CDCl_3$): δ = 7.88-7.82 (m, 8H), 7.70-7.66 (m, 2H), 7.50-7.38 ppm (m, 14H). ^{31}P NMR ($CDCl_3$): δ = 9.16 ppm. IR (ATR): ν = 2965-3090 (st, arC-H), 2173 (st, C≡C), 1194 cm^{-1} (st, P=O). ESI-MS (*m*/*z*): $[M+H]^+$ calcd. for $C_{34}H_{25}O_2P_2$, 527.13; found, 527.13. Anal. calcd. for $C_{34}H_{24}O_2P_2$, C 77.56, H 4.59; found, C 77.09, H 4.50%.

Preparation of [Eu(+tfc)$_3$(*o*-dpeb)]: [Eu(+tfc)$_3$(H_2O)$_2$] (0.37 g, 0.40 mmol) and *o*-dpeb (0.18 g, 0.33 mmol) were dissolved in methanol (10 mL) and refluxed for 18 h. The reaction solution was cooled to room temperature and evaporated, which gave light yellow powder. The obtained powder was washed with diethyl ether and was dried in vacuo. IR (ATR): 2866-2955 (st, arC-H), 2180 (st, C≡C), 1652 (st, C=O), 1183 cm^{-1} (st, P=O). ESI-MS (*m*/*z*) : $[M-tfc]^+$ calcd. for $C_{58}H_{52}EuF_6O_6P_2$, 1173.24; found, 1173.17.

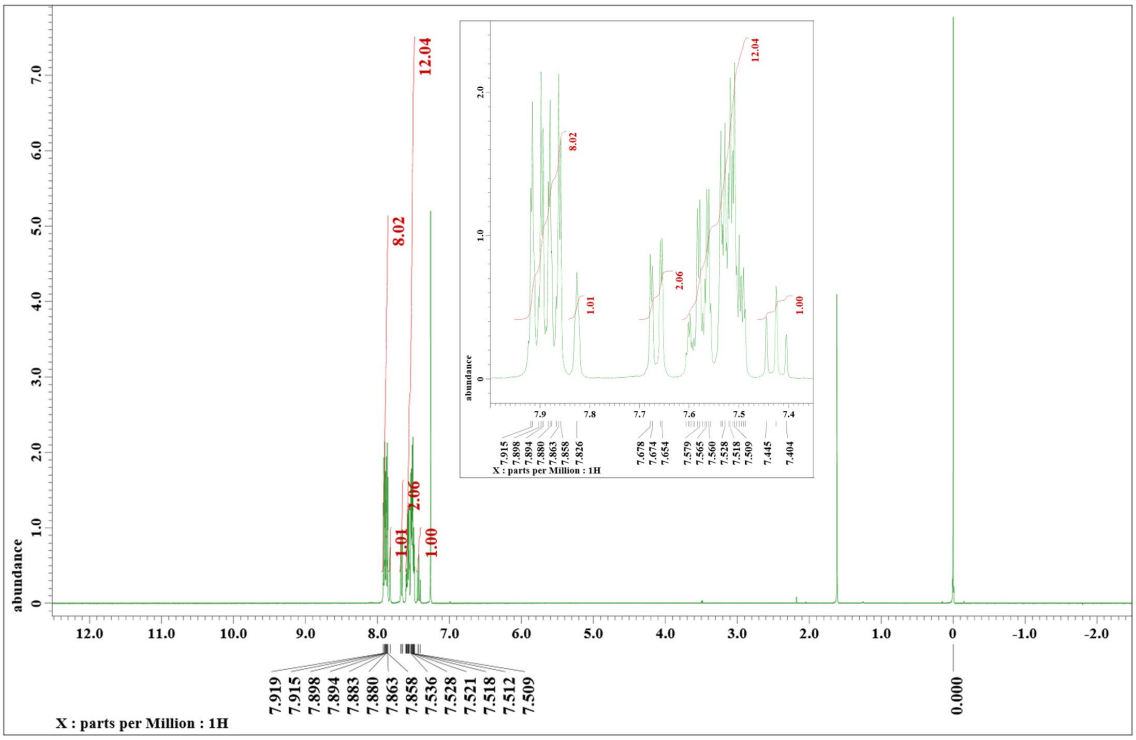

Figure S1. ^{1}H NMR spectra of *m*-dpeb in $CDCl_3$ with TMS as an internal standard (400 MHz).

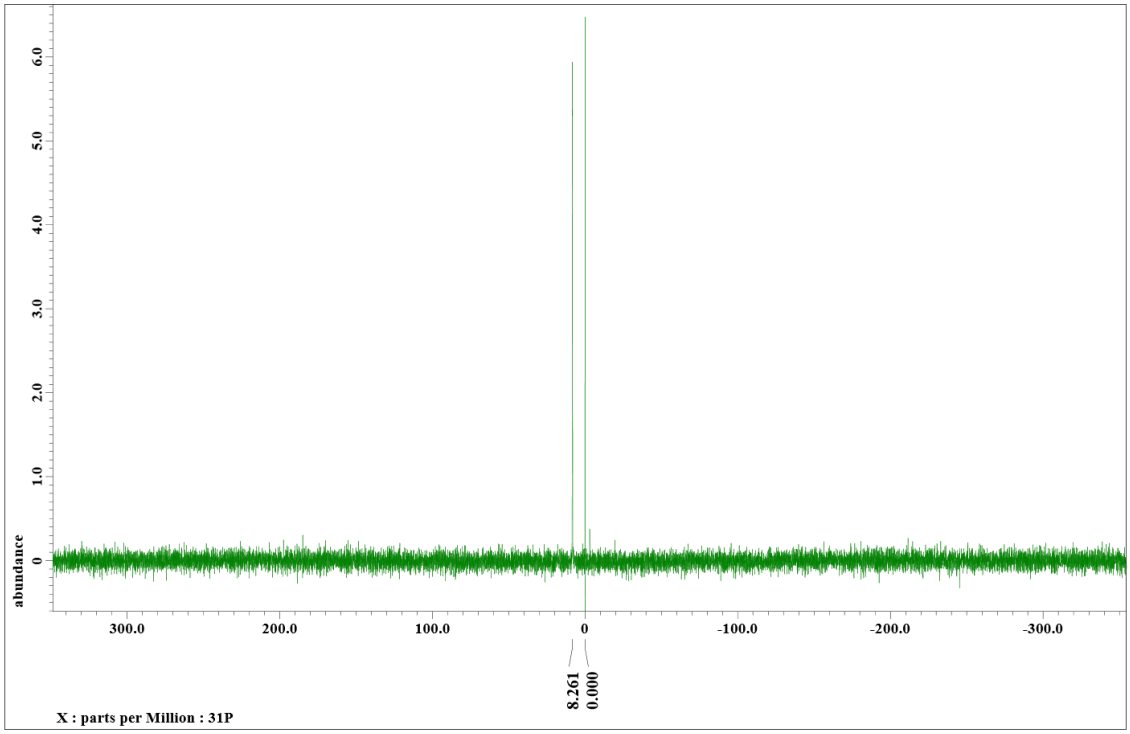

Figure S2. ^{31}P NMR spectrum of *m*-dpeb in $CDCl_3$ with phosphoric acid as an internal standard (162 MHz).

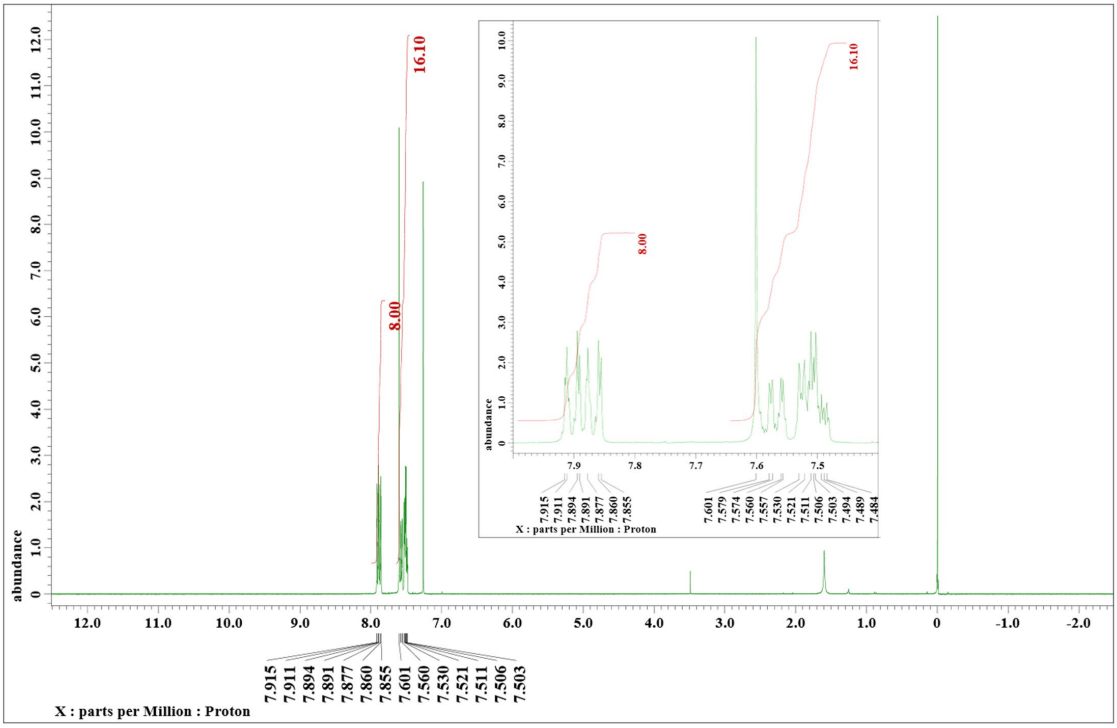

Figure S3. ^{1}H NMR spectra of *p*-dpeb in $CDCl_3$ with TMS as an internal standard (400 MHz).

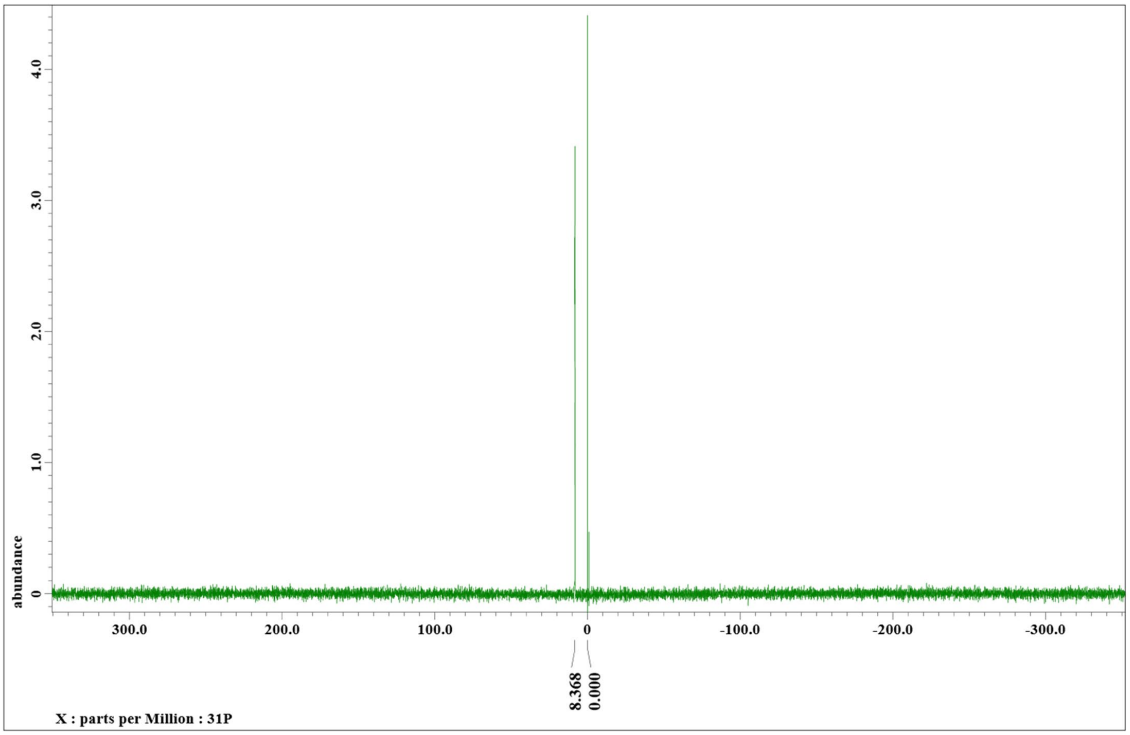

Figure S4. ^{31}P NMR spectrum of *p*-dpeb in $CDCl_3$ with phosphoric acid as an internal standard (162 MHz).

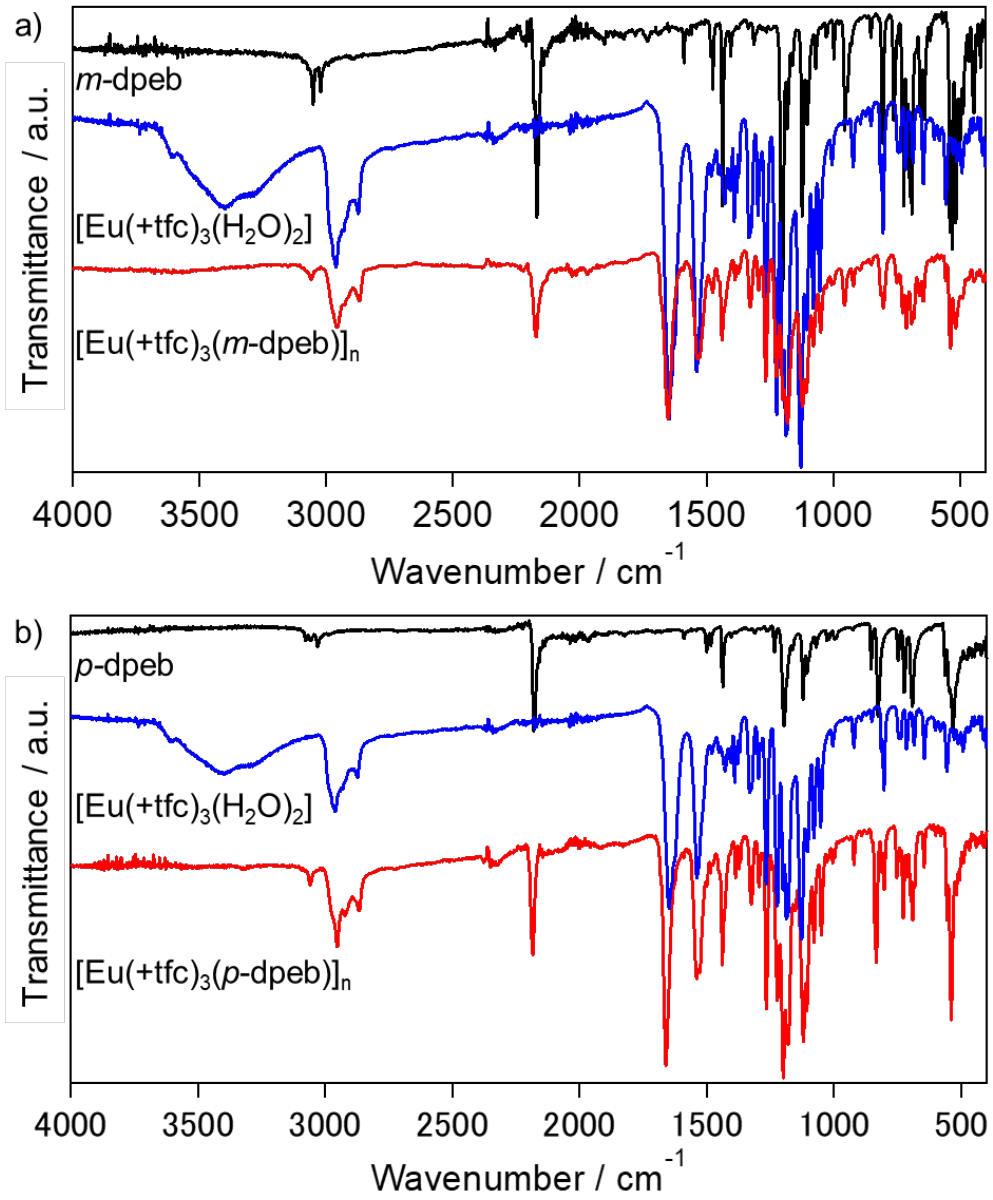

Figure S5. FT-IR spectra of a) *m*-dpeb (black line), $[Eu(+tfc)_3(H_2O)_2]$ (blue line), and $[Eu(+tfc)_3(m\text{-dpeb})]_n$ (red line) and b) *p*-dpeb (black line), $[Eu(+tfc)_3(H_2O)_2]$ (blue line), and $[Eu(+tfc)_3(p\text{-dpeb})]_n$ (red line).

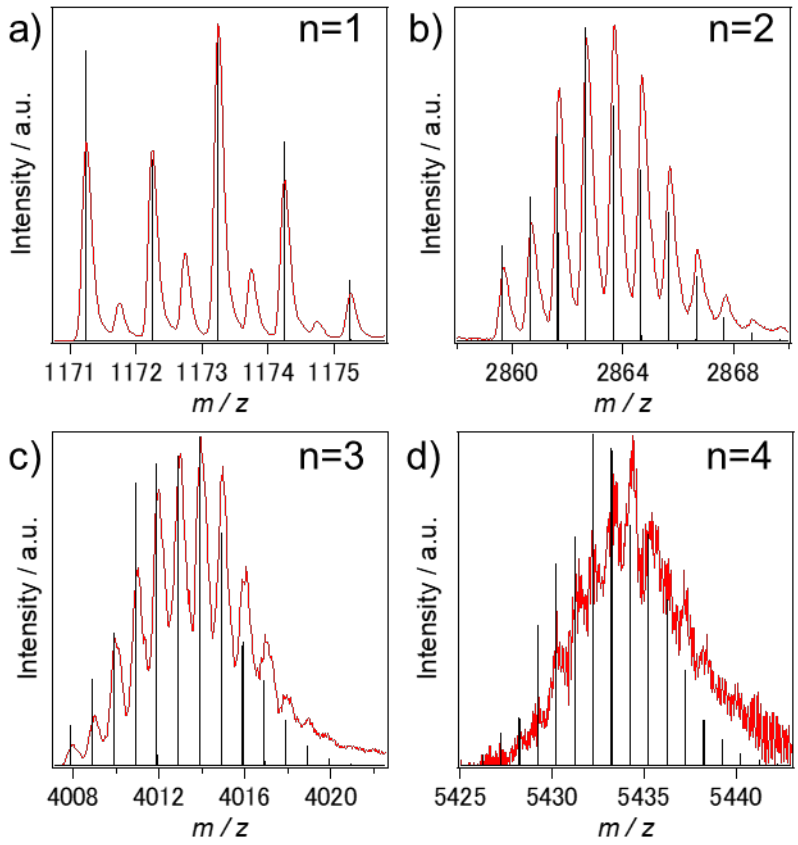

Figure S6. ESI-MS spectra (red) and simulated mass pattern (black) of $[Eu_n(+tfc)_{3n-1}(p\text{-dpeb})_n]^+$ (a) n = 1, b) n = 2, c) n = 3, d) n = 4).

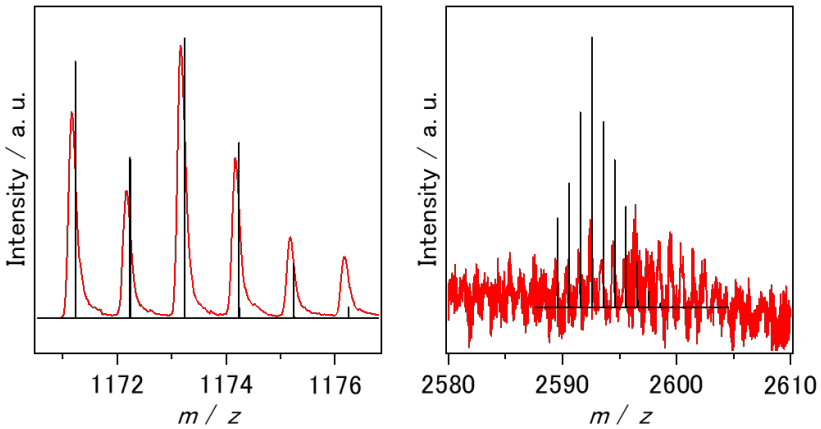

Figure S7. ESI-MS spectra (red) and simulated mass pattern (black) of $[Eu_n(+tfc)_{3n-1}(o\text{-dpeb})_n]^+$ (a) n = 1, b) n = 2).

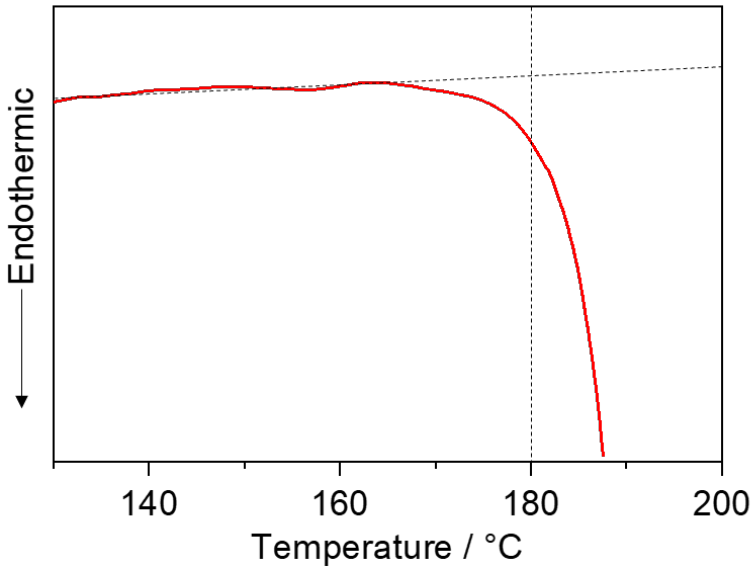

Figure S8. DSC thermograms of $[Eu(+tfc)_3(m\text{-dpeb})]_n$ in a nitrogen atmosphere at a heating and cooling rate of 5 °C min^{-1} expanded the region at 130–200 °C (enlarged view of Figure 3b).

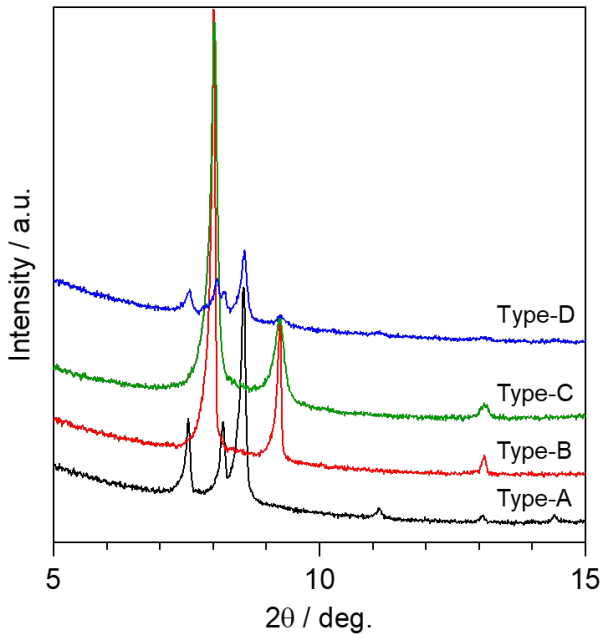

Figure S9. PXRD patterns of $[Eu(+tfc)_3(m\text{-dpeb})]_n$ measured at room temperature after heating treatment (black line: Type-A, red line: Type-B, green line: Type-C, blue line: Type-D).

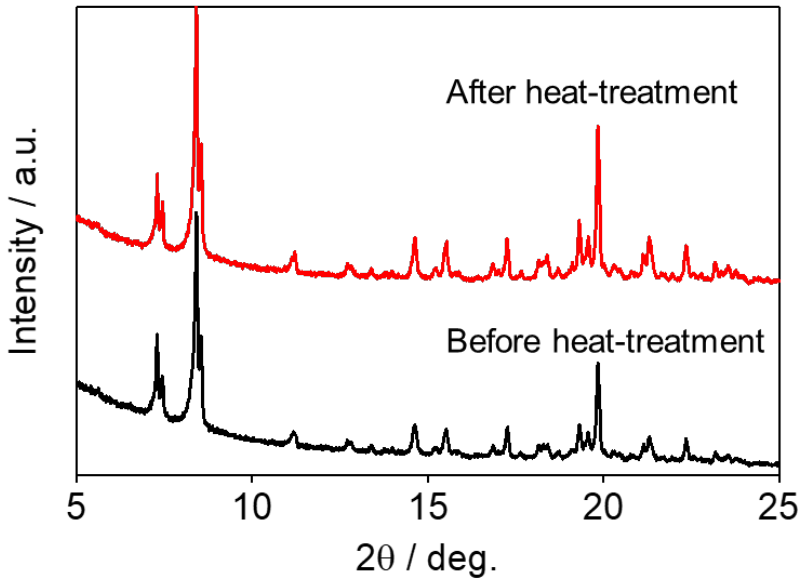

Figure S10. PXRD patterns of $[Eu(+tfc)_3(p\text{-dpeb})]_n$ measured at room temperature before and after heating treatment (black line: without heating, red line: after heating treatment at 200 °C for 30 min and rapid cooling).

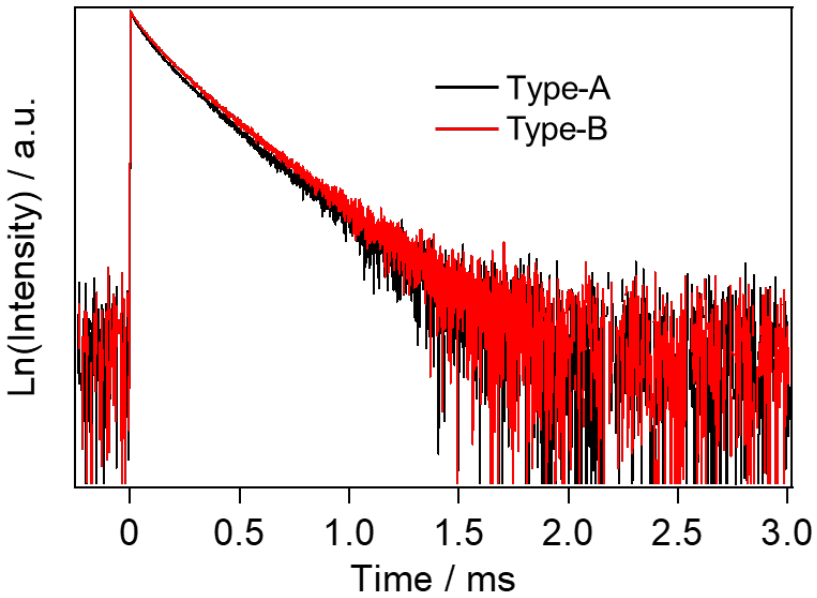

Figure S11. Emission decay profiles (λ_{ex} = 355 nm) of $[Eu(+tfc)_3(m\text{-dpeb})]_n$ measured at room temperature after heating treatment (in powder, black line: Type-A, red line: Type-B).

Temperature-dependent emission lifetime measurements

To estimate the effect of energy transfer from Eu(III) to the LMCT states in Type-A and Type-B, the temperature-dependent emission lifetimes in the solid state were measured in the range of 100–350 K (Figure S12). The emission decay profiles measured at 100–250 K displayed a single exponential decay, whereas double exponential decays were observed in the higher temperature range. The double exponential decay might arise from the two emission sites of the Eu(III) ion. Each emission sites exhibit different emission lifetime in the higher temperature range because of the difference in LMCT contribution.

The relationship between the average emission lifetime and temperature is shown in Figure S13. Based on the temperature-dependent emission lifetimes, the back energy transfer rate constants (k_{BEnT}) were estimated using kinetic analysis. The temperature-dependence of k_{BEnT} was expected to follow an Arrhenius-type equation, which is defined by the following equation:[S2-S4]

$$\ln\left(\frac{1}{\tau_{\mathrm{obs}}}-\frac{1}{\tau_{100\mathrm{K}}}\right)=\ln k_{\mathrm{BEnT}}=\ln A-\frac{\Delta E_{\mathrm{a}}}{RT}, \quad \text{(S1)}$$

where τ_{obs}, $\tau_{100\mathrm{K}}$, A, ΔE_{a}, R, and T are the observed emission lifetime, standard emission lifetime at 100 K, frequency factor, activation energy, gas constant, and temperature, respectively. In the 4f-4f transitions in Eu(III) compounds, the vibrational deactivation of 4f-4f transition is usually insensitive to the temperature because of the large energy gap between excited and ground states[S5]. From the Arrhenius analysis, the non-radiative rate factor in k_{BEnT} is only depended on the back energy transfer process from Eu(III) to the LMCT states. Arrhenius plots of Type-A and Type-B are shown in Figure S14, and the calculated ΔE_{a} and A values are summarized in Table S1. The Arrhenius plots were well fitted to the equation (S1) with high coefficient of determination (R^2 = 0.995 (Type-A), and 0.998 (Type-B)), suggesting the single temperature-dependent quenching state. The large difference in the ΔE_{a} and A values between Type-A and Type-B indicates that the LMCT characteristics can be affected by the molecular orientation change based on the phase-transition.

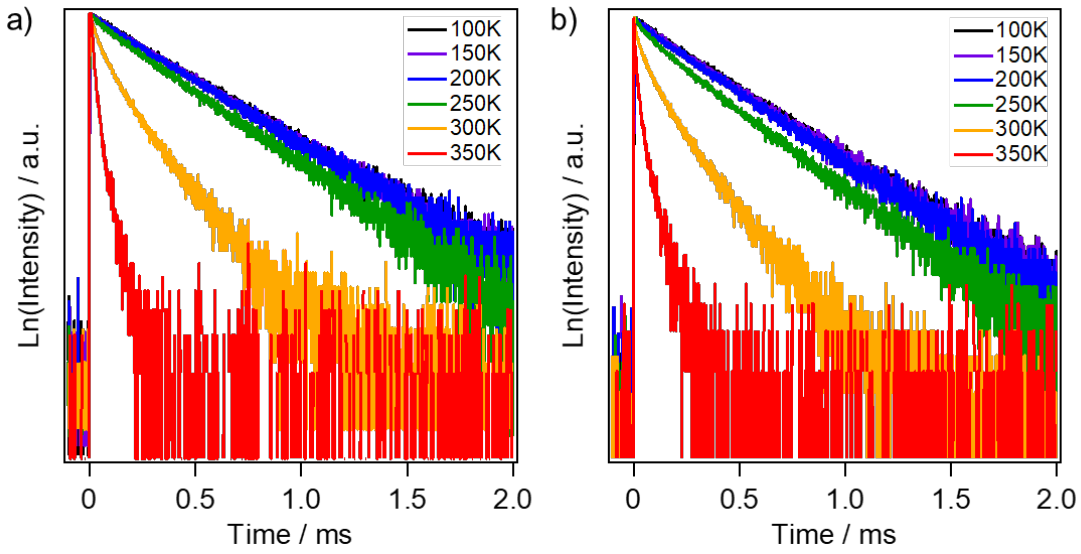

Figure S12. Temperature-dependent emission decay profiles of a) Type-A and b) Type-B (λ_{ex} = 355 nm, λ_{em} = 612 nm).

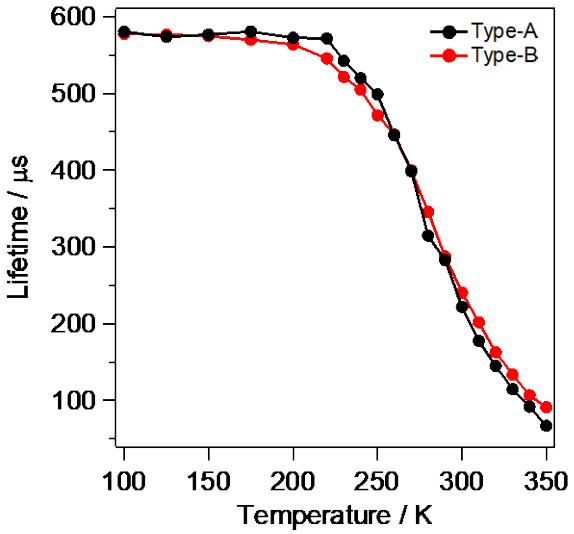

Figure S13. Temperature-dependent emission lifetime of $[Eu(+tfc)_3(m\text{-dpeb})]_n$ (black line: Type-A, red line: Type-B, λ_{ex} = 355 nm, λ_{em} = 612 nm).

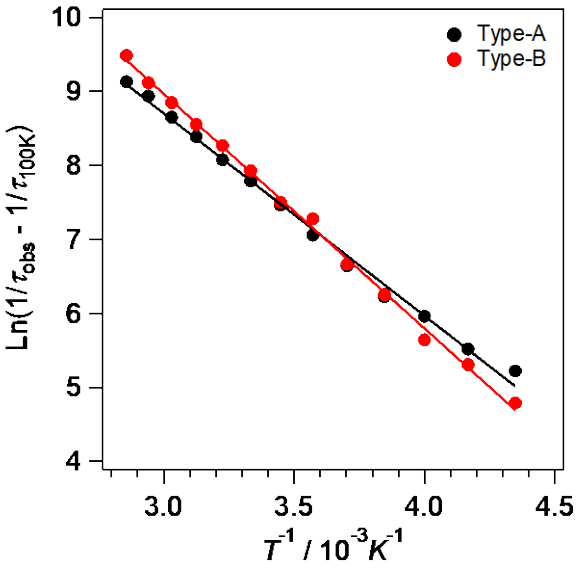

Figure S14. Arrhenius plots of $[Eu(+tfc)_3(m\text{-dpeb})]_n$ (black: Type-A, red: Type-B).

Table S1. Arrhenius parameters of $[Eu(+tfc)_3(m\text{-dpeb})]_n$.

	ΔE_a / cm^{-1}	A / s^{-1}
Type-A	2,200	1.1×10^8
Type-B	1,880	2.0×10^7

Amorphization by additive phosphine oxide ligand to Eu(III) coordination polymers

Monodentate phosphine oxide tppo (tppo: triphenylphosphine oxide) was used for amorphization of the coordination polymer. The tppo molecules were added to the Eu(III) coordination polymers using the following procedure.

The Eu(III) coordination polymer (1 eq.) and tppo molecules (2 eq.) were ground using an agate mortar for 5 min. For comparison, pure Type-A and Type-B were also ground before PXRD measurements. The PXRD patterns before and after adding the tppo ligand to the Type-A and -B coordination polymers are shown in Figure S15. The mixture of Type-A and tppo (Type-A+tppo) shows broad signals at approximately $2\theta = 8°$, although tppo and pure Type-A show characteristically sharp peaks. The mixture of Type-B and tppo (Type-B+tppo) exhibits a decrease in crystallinity. The typical molecular orientation of chiral Eu(III) coordination polymers disappeared with the addition of TPPO molecules.

The emission and CPL spectra of the chiral Eu(III) coordination polymers before and after adding the tppo molecule are shown in Figure S16. The emission spectral shape with Stark splitting remains unchanged by the addition of tppo. The coordination geometries around Eu(III) ions are unaffected by the addition of tppo molecules. On the other hand, the CPL intensities of these coordination polymers change substantially. After the addition of TPPO molecules, the g_{CPL} value of Type-A+tppo (−0.076) was similar to that of Type-B+tppo (−0.077), although the g_{CPL} value of pure Type-A was three times larger than that of pure Type-B. These phenomena might occur owing to a breakage in the molecular orientation, which affects the CPL properties of Eu(III) coordination polymers. These results indicate that the characteristic macroscopic structures of Type-A and Type-B effectively affected the CPL properties of chiral Eu(III) coordination polymers in a solid system.

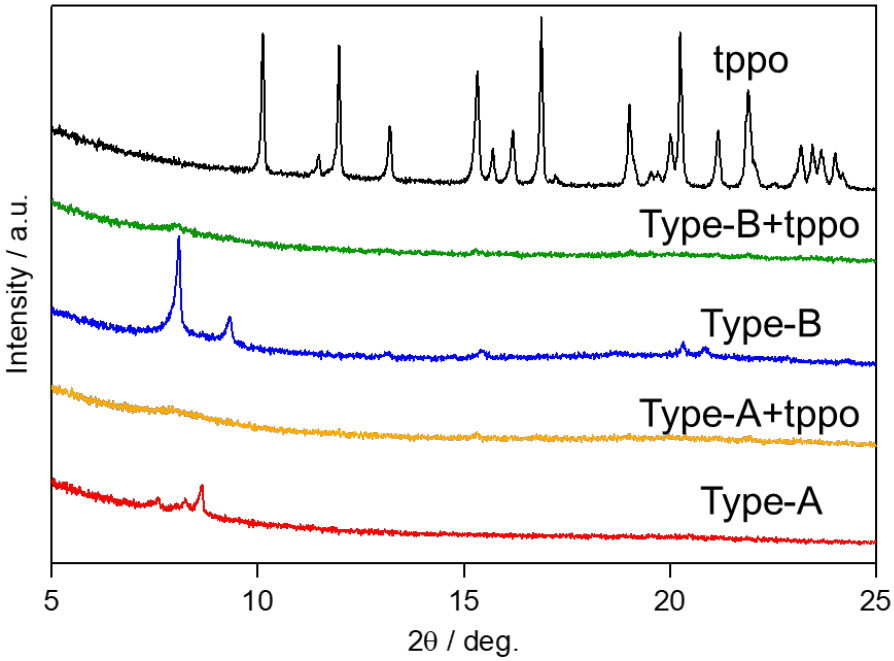

Figure S15. PXRD patterns of $[Eu(+tfc)_3(m\text{-dpeb})]_n$ measured at room temperature after adding tppo molecule (black line: tppo, red line: Type-A, yellow line: Type-A+tppo, blue line: Type-B, green line: Type-B+tppo).

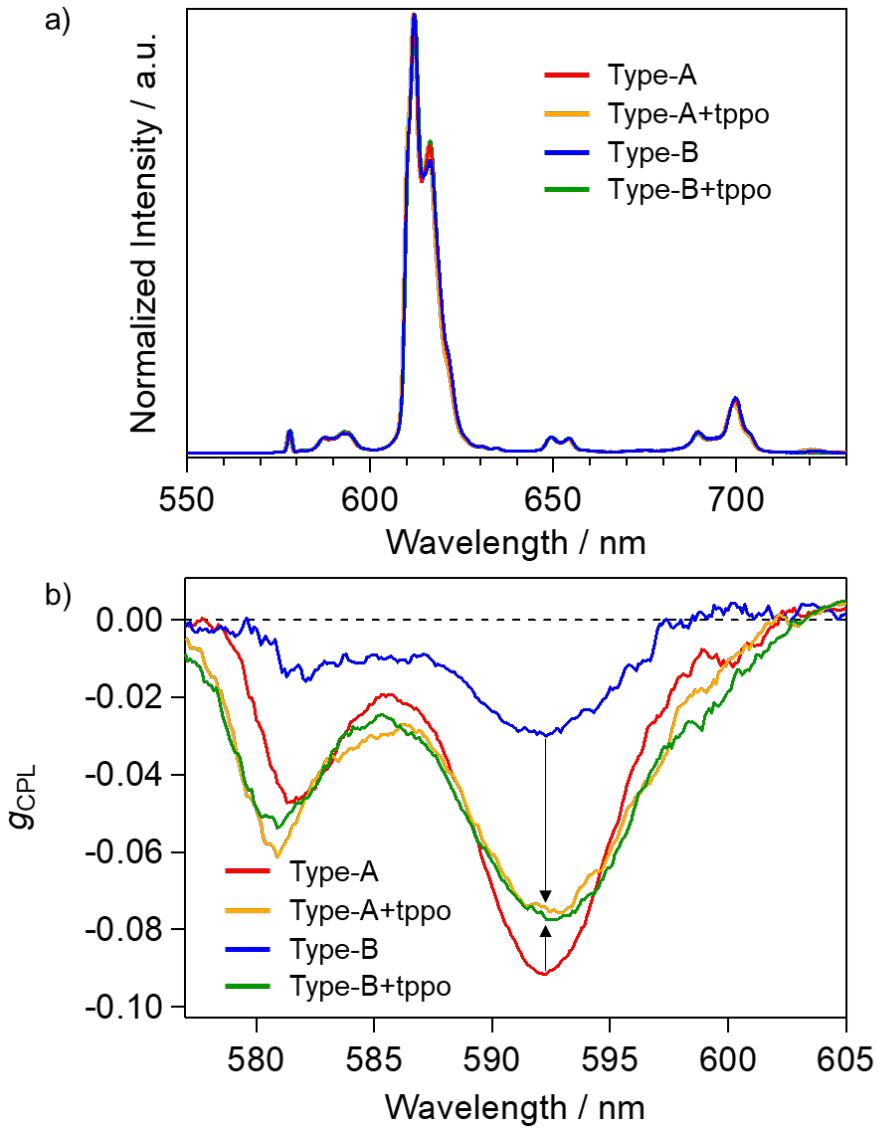

Figure S16. (a) Emission and (b) g_{CPL} spectra of $[Eu(+tfc)_3(m\text{-dpeb})]_n$ measured at room temperature after adding tppo molecule (λ_{ex} = 360 nm, black line: tppo, red line: Type-A, yellow line: Type-A+tppo, blue line: Type-B, green line: TypeB+tppo).

DFT calculations

Table S2. The excitation energies of $Eu(+tfc)_3(tppo)_2$ dimer model ($d_{Eu\text{-}Eu}$ = 13 Å) obtained by TD-DFT calculation.

excited state	excitation energy / cm^{-1}	oscillator strength	largest configuration	character	splitting energy gap (ΔE_{split}) / cm^{-1}
1	1047	0.0000	HOMO−128 → LUMO+1 (α)	4f-4f	7
2	1054	0.0000	HOMO−132 →LUMO (α)	4f-4f	
3	1776	0.0000	HOMO−148 → LUMO+1 (α)	4f-4f	2
4	1778	0.0000	HOMO−157 →LUMO (α)	4f-4f	
5	1972	0.0000	HOMO−148 → LUMO+1 (α)	4f-4f	4
6	1977	0.0000	HOMO−149 →LUMO (α)	4f-4f	
7	2429	0.0000	HOMO−114 → LUMO+1 (α)	4f-4f	7
8	2436	0.0000	HOMO−120 →LUMO (α)	4f-4f	
9	3432	0.0000	HOMO−100 →LUMO (α)	4f-4f	5
10	3437	0.0000	HOMO−98 → LUMO+1 (α)	4f-4f	
11	3671	0.0000	HOMO−117 →LUMO (α)	4f-4f	2
12	3674	0.0000	HOMO−110 → LUMO+1 (α)	4f-4f	
13	12100	0.0055	HOMO−1 →LUMO (α)	LMCT	196
14	12297	0.0059	HOMO → LUMO+1 (α)	LMCT	
15	15682	0.0013	HOMO−3 →LUMO (α)	LMCT	191
16	15873	0.0012	HOMO−2→ LUMO+1 (α)	LMCT	
17	16409	0.0002	HOMO−4→ LUMO+1 (α)	LMCT	554
18	16963	0.0002	HOMO−5 →LUMO (α)	LMCT	
19	20161	0.0055	HOMO−8 →LUMO (α)	LMCT	184
20	20345	0.0058	HOMO−7→ LUMO+1 (α)	LMCT	
21	20592	0.0130	HOMO−6→ LUMO+1 (α)	LMCT	93
22	20685	0.0120	HOMO−9 →LUMO (α)	LMCT	

Table S3. The excitation energies of $Eu(+tfc)_3(tppo)_2$ dimer model ($d_{Eu\text{-}Eu}$ = 14 Å) obtained by TD-DFT calculation.

excited state	excitation energy / cm^{-1}	oscillator strength	largest configuration	character	splitting energy gap (ΔE_{split}) / cm^{-1}
1	1048	0.0000	HOMO−128 → LUMO+1 (α)	4f-4f	8
2	1056	0.0000	HOMO−134 →LUMO (α)	4f-4f	
3	1777	0.0000	HOMO−148 → LUMO+1 (α)	4f-4f	2
4	1779	0.0000	HOMO−156 →LUMO (α)	4f-4f	
5	1974	0.0000	HOMO−144 → LUMO+1 (α)	4f-4f	4
6	1978	0.0000	HOMO−149 →LUMO (α)	4f-4f	
7	2428	0.0000	HOMO−114 → LUMO+1 (α)	4f-4f	6
8	2434	0.0000	HOMO−127 →LUMO (α)	4f-4f	
9	3435	0.0000	HOMO−100 →LUMO (α)	4f-4f	4
10	3438	0.0000	HOMO−98 → LUMO+1 (α)	4f-4f	
11	3673	0.0000	HOMO−116 →LUMO (α)	4f-4f	2
12	3674	0.0000	HOMO−110 → LUMO+1 (α)	4f-4f	
13	12075	0.0056	HOMO−1 →LUMO (α)	LMCT	156
14	12232	0.0059	HOMO → LUMO+1 (α)	LMCT	
15	15707	0.0013	HOMO−3 →LUMO (α)	LMCT	158
16	15865	0.0012	HOMO−2→ LUMO+1 (α)	LMCT	
17	16486	0.0002	HOMO−4→ LUMO+1 (α)	LMCT	437
18	16923	0.0002	HOMO−5 →LUMO (α)	LMCT	
19	20143	0.0056	HOMO−8 →LUMO (α)	LMCT	144
20	20288	0.0059	HOMO−7→ LUMO+1 (α)	LMCT	
21	20620	0.0129	HOMO−6→ LUMO+1 (α)	LMCT	62
22	20683	0.0116	HOMO−9 →LUMO (α)	LMCT	

Table S4. The excitation energies of $Eu(+tfc)_3(tppo)_2$ dimer model ($d_{Eu\text{-}Eu}$ = 15 Å) obtained by TD-DFT calculation.

excited state	excitation energy / cm^{-1}	oscillator strength	largest configuration	character	splitting energy gap (ΔE_{split}) / cm^{-1}
1	1049	0.0000	HOMO−129 → LUMO+1 (α)	4f-4f	8
2	1056	0.0000	HOMO−133 →LUMO (α)	4f-4f	
3	1778	0.0000	HOMO−148 → LUMO+1 (α)	4f-4f	2
4	1780	0.0000	HOMO−155 →LUMO (α)	4f-4f	
5	1975	0.0000	HOMO−145 → LUMO+1 (α)	4f-4f	4
6	1979	0.0000	HOMO−149 →LUMO (α)	4f-4f	
7	2428	0.0000	HOMO−117 → LUMO+1 (α)	4f-4f	5
8	2433	0.0000	HOMO−123 →LUMO (α)	4f-4f	
9	3436	0.0000	HOMO−103 →LUMO (α)	4f-4f	2
10	3439	0.0000	HOMO−98 → LUMO+1 (α)	4f-4f	
11	3673	0.0000	HOMO−116 →LUMO (α)	4f-4f	1
12	3674	0.0000	HOMO−110 → LUMO+1 (α)	4f-4f	
13	12062	0.0057	HOMO−1 →LUMO (α)	LMCT	127
14	12189	0.0060	HOMO → LUMO+1 (α)	LMCT	
15	15721	0.0013	HOMO−3 →LUMO (α)	LMCT	134
16	15855	0.0012	HOMO−2→ LUMO+1 (α)	LMCT	
17	16544	0.0002	HOMO−4→ LUMO+1 (α)	LMCT	355
18	16899	0.0002	HOMO−5 →LUMO (α)	LMCT	
19	20135	0.0057	HOMO−8 →LUMO (α)	LMCT	115
20	20249	0.0059	HOMO−7→ LUMO+1 (α)	LMCT	
21	20638	0.0128	HOMO−6→ LUMO+1 (α)	LMCT	43
22	20681	0.0112	HOMO−9 →LUMO (α)	LMCT	

a) HOMO−157

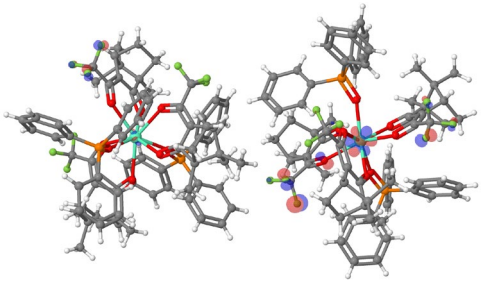

b) HOMO−149

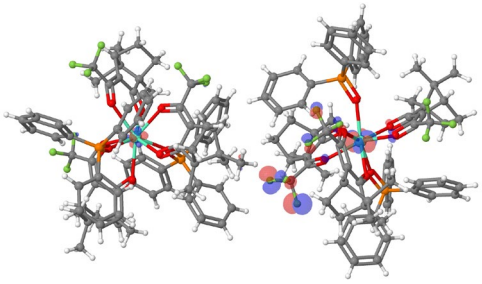

c) HOMO−148

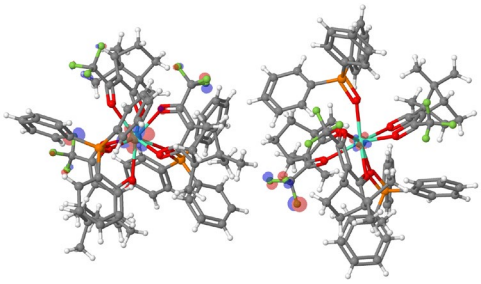

d) HOMO−132

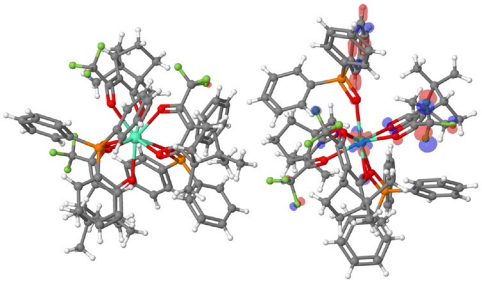

e) HOMO−128

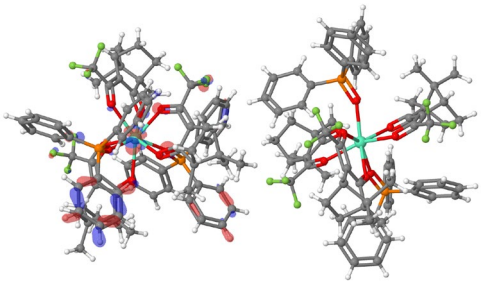

f) HOMO−120

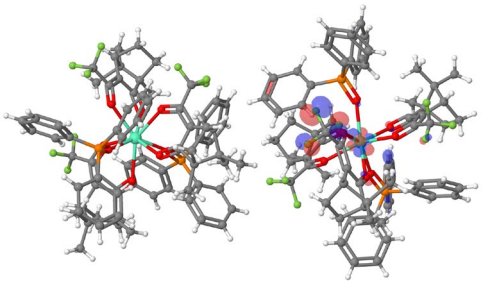

g) HOMO−117

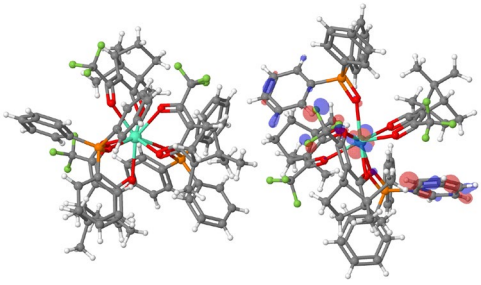

h) HOMO−114

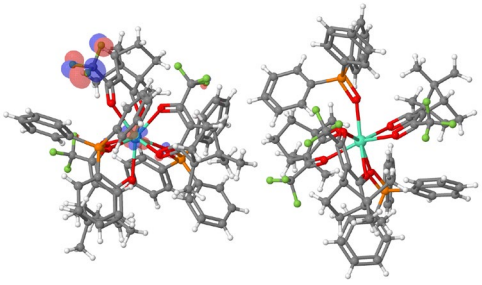

i) HOMO−110

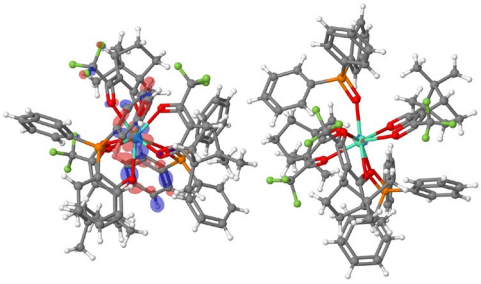

j) HOMO−100

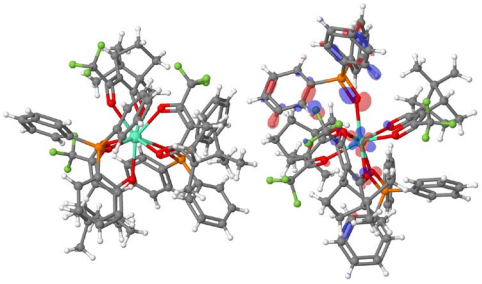

k) HOMO−95

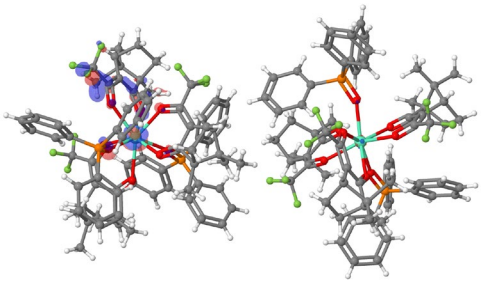

l) HOMO−9

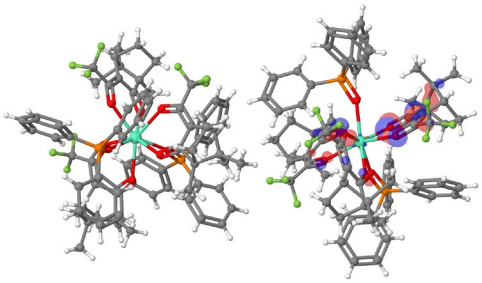

m) HOMO−8

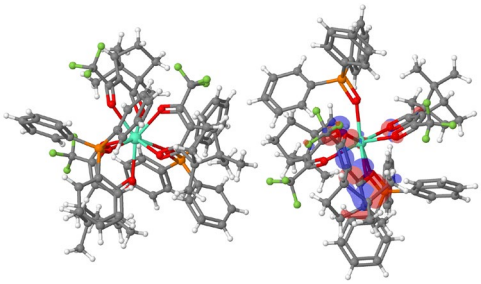

n) HOMO−7

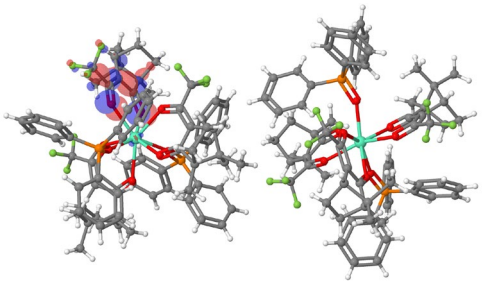

o) HOMO−6

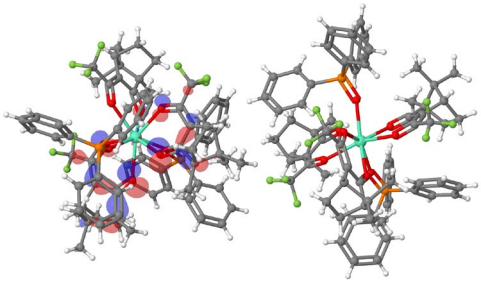

p) HOMO−5

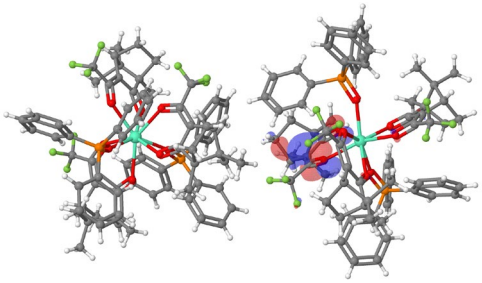

q) HOMO−4

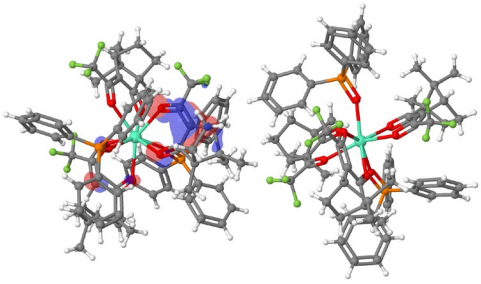

r) HOMO−3

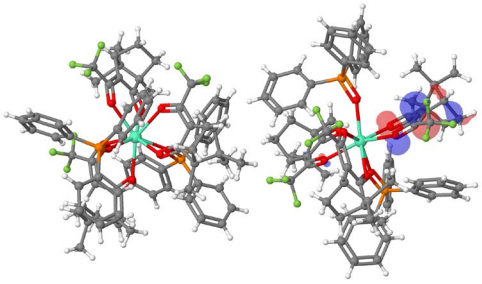

s) HOMO−2

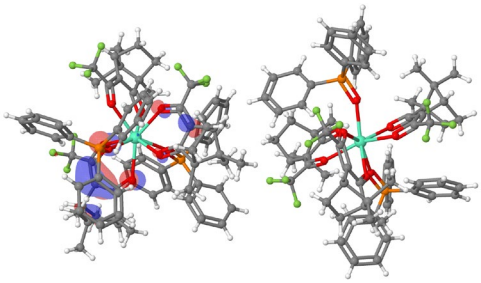

t) HOMO−1

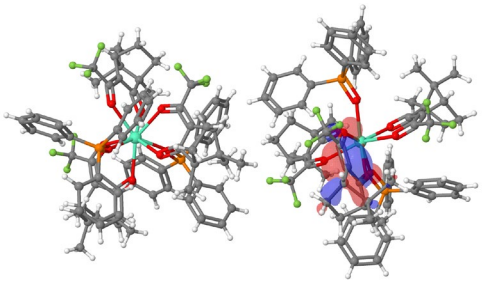

u) HOMO

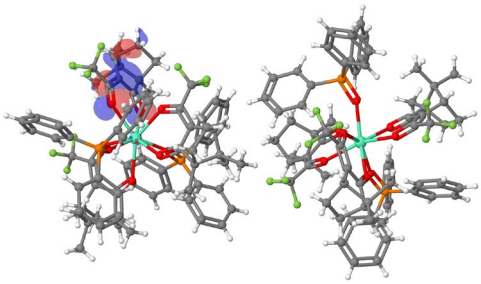

v) LUMO

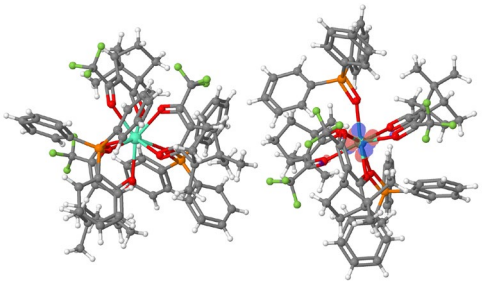

w) LUMO+1

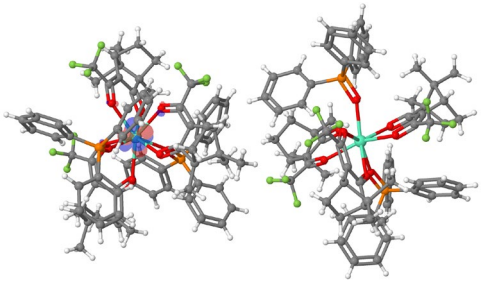

Figure S17. Selected α-spin molecular orbitals of Eu(+tfc)$_3$(tppo)$_2$ dimer model ($d_{Eu\text{-}Eu}$ = 12.79Å).

The TD-DFT calculations were also conducted for the modified dimer model of [Eu(+tfc)$_3$(tppo)$_2$] rotating the O1-Eu1-Eu2 angle of the original dimer model to $A_{O1\text{-}Eu1\text{-}Eu2}$ = 180, 150, 120, and 90° (Figure S18a). The $d_{Eu\text{-}Eu}$ of these model were fixed to 14 Å. Based on the calculation data, the magnitudes of the $|\vec{\mu}|$ in the excited states 13–22 (LMCT transitions) was dependent on the $A_{O1\text{-}Eu1\text{-}Eu2}$ (Figure S18b). The LMCT states were affected by not only the distance but also the direction between the Eu units.

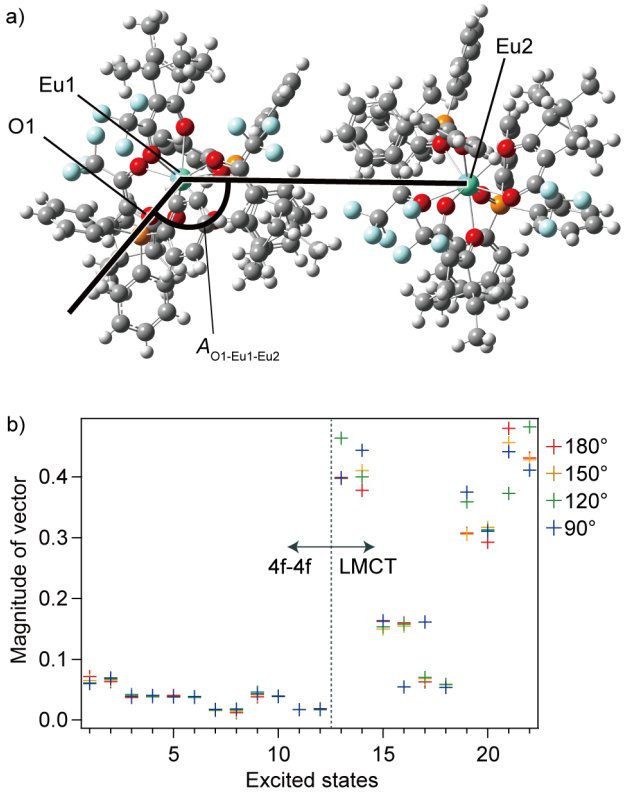

Figure S18. a) Molecular structure of Eu(+tfc)$_3$(tppo)$_2$ dimer model. b) Magnitude of transition electric dipole moment vectors ($|\vec{\mu}|$) in 4f-4f or LMCT excited states.

References

(S1) Hirai, Y.; Nakanishi, T.; Kitagawa, Y.; Fushimi, K.; Seki, T.; Ito, H.; Fueno, H.; Tanaka, K.; Satoh, T.; Hasegawa, Y. Luminescent Coordination Glass: Remarkable Morphological Strategy for Assembled Eu(III) Complexes. *Inorg. Chem.* **2015**, *54*, 4364–4370.

(S2) Olofsson, J.; Önfelt, B.; Lincoln, P. Three-State Light Switch of $[Ru(Phen)_2dppz]^{2+}$: Distinct Excited-State Species with Two, One, or No Hydrogen Bonds from Solvent. *J. Phys. Chem. A* **2004**, *108*, 4391–4398.

(S3) Miyata, K.; Konno, Y.; Nakanishi, T.; Kobayashi, A.; Kato, M.; Fushimi, K.; Hasegawa, Y. Chameleon Luminophore for Sensing Temperatures: Control of Metal-to-Metal and Energy Back Transfer in Lanthanide Coordination Polymers. *Angew. Chem. Int. Ed.* **2013**, *52*, 6413–6416.

(S4) Yamamoto, M.; Kitagawa, Y.; Nakanishi, T.; Fushimi, K.; Hasegawa, Y. Ligand-Assisted Back Energy Transfer in Luminescent Tb^{III} Complexes for Thermosensing Properties. *Chem. Eur. J.* **2018**, *24*, 17719–17726.

(S5) Berry, M. T.; May, P . S.; Xu, H. Temperature Dependence of the Eu^{3+} $^5D_0$ Lifetime in Europium Tris(2,2,6,6-tetramethyl-3,5-heptanedionato). *J. Phys. Chem.* **1996**, *100*, 9216–9222.